2010

# Some Possible Approaches for Improving the Energy Density of Li-air Batteries

Petru Andrei, Jim Zheng, Mary Hendrickson, and Edward J. Plichta

# Some possible approaches for improving the energy density of Li-air batteries

P. Andrei[(a)], J.P. Zheng[(a)(b)], M. Hendrickson[(c)], and E.J. Plichta[(c)]

[(a)]Department of Electrical and Computer Engineering, Florida A&M University and Florida State University, Tallahassee, FL 32310

[(b)]Center for Advanced Power Systems, Florida State University, Tallahassee, FL 32310

[(c)]U.S. Army CERDEC, Fort Monmouth, NJ 07703

**Abstract.** A physics-based model is proposed for the simulation of Li-air batteries. The model is carefully calibrated against published data and is used to simulate standard Li-air batteries with nonaqueous (organic) electrolyte. It is shown that the specific capacity is mainly limited by the oxygen diffusion length which is a function of the oxygen diffusivity in the electrolyte and the discharge current density. Various approaches to increase the specific capacity of the cathode electrode and the energy density of Li-air batteries are discussed. It is shown that, in order to increase the specific capacity and energy density, it is more efficient to use a nonuniform catalyst that enhances the reaction rate only at the separator-cathode interface than a catalyst uniformly distributed. Using uniformly distributed catalysts will enhance the current and power density of the cell but will not increase significantly the specific capacity and energy density. It is also shown that the specific capacity and energy density can be increased by suppressing the reaction rate at the oxygen-entrance interface in order to delay the pinch-off of the conduction channel in this region. Other possibilities to enhance the energy density such as using solvents with high oxygen solubility and diffusivity, and partly wetted electrodes are discussed.

Li-air batteries have attracted much attention recently because of their relatively high theoretical energy densities compared to other batteries. The high theoretical energy density of Li-air batteries makes these batteries suitable for applications requiring light power sources such as portable electronic devices, unmanned aerial vehicles, or any other equipment where air is present. Despite their high maximum energy density,[1-3] current Li-air batteries typically achieve only a fraction of the maximum theoretical energy density. In this article we develop a physics-based model based on a drift-diffusion approach to simulate Li-air batteries with nonaqueous electrolyte and propose battery structures with improved energy density.

Li-air batteries with nonaqueous electrolyte are usually composed of a Li metallic anode, a solid separator, and a porous carbon cathode filled with organic electrolyte (see Fig. 1). External air is allowed to penetrate the pores of the cathode, diffuse through the electrolyte, and react with the Li ions according to reaction:

$$2\,\mathrm{Li}^{+} + \mathrm{O}_2 + 2\,\mathrm{e}^{-} \rightarrow \mathrm{Li}_2\mathrm{O}_2\,. \qquad (1)$$

The $Li_2O_2$ reaction product is insoluble in the electrolyte and deposits on the solid surface of the cathode as shown in Fig. 2. As noted by Reed et al.[4] the formation of lithium peroxide, which fills in the channels and interrupts the flow on $O_2$ in the cathode, constitutes the main reason for the relatively short life of current Li-air batteries. Also, the relatively low value of the diffusion coefficient of $O_2$ in the electrolyte significantly reduces the power density of these batteries. It was concluded by a number of authors that in order to enhance the power density of Li-air batteries one needs to increase either the $O_2$ diffusivity and concentration in the electrolyte or the gaseous oxygen partial pressure.[5, 6] It is shown in this article that, although some of these approaches are appropriate to enhance the power density of Li-air batteries they are not always very efficient in increasing the energy density of these batteries.

It has been noted in the literature that lithium oxide ($Li_2O$) can also be formed at the cathode as a results of the Li oxidation. This formation can also be taken into consideration in our modeling by carefully calibrating the parameters of the models used (e.g. molecular mass, mass density, etc.). However, the simulations presented in this article assume that lithium peroxide is the main reaction product at the cathode.

The article is structured as follows. In the first section we summarize the model that we use for the simulation of Li-air batteries. This model is similar to already existing models for Li-ion

batteries[7-9], however it also takes into consideration the oxygen diffusion and reaction rate at the cathode. The formation of the $Li_2O_2$ at the cathode is modeled by using a model similar to the one developed by Sandhu et al.[6] In the second section of the article, we present the numerical algorithm and sample simulation results. Then, we discuss about possible approaches to improve the specific capacity of the cathode electrode and the energy density of Li-air batteries, after which we conclude.

## Model development

*Basic equations* –The mathematical description of Li-air batteries should include accurate models for the lithium-ion and oxygen diffusion inside the cell, the electron conductivity of the carbon cathode, $Li_2O_2$ formation and deposition at the cathode, the porosity change inside the cathode, and rate equations for reaction (1) and for the Li ion formation ($\mathrm{Li} \rightarrow \mathrm{Li}^+ + \mathrm{e}^-$). In this work we use the theory of concentrated solutions[10] to model the $Li^+$ and oxygen diffusion and drift in the anode protective layer (APL), separator, and cathode electrolyte. We also assume a binary monovalent electrolyte and no convection. The electrostatic potential of Li ions, $\phi_{Li}$ is assumed to satisfy the following drift-diffusion equation:

$$\nabla \cdot \left( \kappa_{eff} \nabla \phi_{Li} + \kappa_D \nabla \ln c_{Li} \right) - R_C = 0 , \tag{2}$$

where $\kappa_{eff}$ is the effective electric conductivity of $Li^+$ in the solid or liquid electrolyte, $\kappa_D$ is the diffusional conductivity, $c_{Li}$ is the concentration of the lithium electrolyte (which is equal to the concentration of $Li^+$), and $R_C$ is the oxygen conversion rate, which is equal to zero in the APL and separator and is positive in the cathode. The concentration of $Li^+$ satisfies:[10]

$$\frac{\partial \left( \varepsilon c_{Li} \right)}{\partial t} = \nabla \cdot \left( D_{Li,eff} \nabla c_{Li} \right) - \frac{1 - t^+}{F} R_C - \frac{\boldsymbol{I}_{Li} \cdot \nabla t_+}{F} , \tag{3}$$

where $\varepsilon$ is the porosity, $D_{Li,eff}$ is the effective electrolyte diffusion coefficient, $t^+$ is the transference number, $F = 96{,}487$ C/mol is the Faraday constant, and $\boldsymbol{I}_{Li} = -\kappa_{eff} \nabla \phi_{Li} - \kappa_D \nabla \ln c_{Li}$ is the electrolyte density current. The oxygen concentration satisfies the following diffusion equation:

$$\frac{\partial\left(\varepsilon c_{O_2}\right)}{\partial t}=\nabla\cdot\left(D_{O_2,eff}\nabla c_{O_2}\right)-\frac{R_C}{2F}, \tag{4}$$

where $D_{O_2,eff}$ is the effective diffusion constant of the oxygen.

It is important to note that $\kappa_{eff}$, $\kappa_D$, $D_{Li,eff}$, $t^+$, and $D_{O_2,eff}$ in the above equations are material dependent parameters that usually depend on the tortuosity (through porosity) and on the $Li^+$ and oxygen concentration. These parameters should be carefully calibrated for each region (i.e. separator, APL, and cathode electrolyte) in order to model the battery accurately. Following what is usually done in the literature, we assume that all effective quantities can be written in terms of the porosity using Bruggeman correlations as:[10]

$$D_{Li,eff}=\varepsilon^{\beta_{Li}-1}D_{Li}, \tag{5}$$

$$D_{O_2,eff}=\varepsilon^{\beta_{O2}-1}D_{O_2}, \tag{6}$$

$$\kappa_{eff}=\varepsilon^{\beta}\kappa, \tag{7}$$

where $D_{Li}$, $D_{O_2}$ and $\kappa$ are the diffusion coefficients of electrolyte, $O_2$, and the electric conductivity of Li, respectively. Constants $\beta_{Li}$, $\beta_{O2}$, and $\beta$ are the Bruggeman coefficients for electrolyte diffusion, $O_2$ diffusion, and electrolyte conductivity, respectively. The diffusional conductivity is considered as:[8]

$$\kappa_D=\frac{2RT\kappa_{eff}\left(t^+-1\right)}{F}\left(1+\frac{\partial f}{\partial\ln c_{Li}}\right), \tag{8}$$

where $R=8.314$ J/mol K is the universal gas constant, and $T$ is the absolute temperature. In our simulations $\frac{\partial f}{\partial\ln c_{Li}}$ is approximated to zero.

Besides equations (1)-(3) that are solved in all three regions (APL, separator, and cathode), the following two equations are solved in the cathode region to compute the potential of electrons ($\phi$) and the change in the local porosity $\varepsilon$:

$$\nabla\cdot\left(\sigma_{eff}\nabla\phi\right)+R_C=0, \tag{9}$$

$$\frac{\partial \varepsilon}{\partial t} = -R_C \frac{M_{Li_2O_2}}{2F\rho_{Li_2O_2}}, \tag{10}$$

where $M_{Li_2O_2}$ and $\rho_{Li_2O_2}$ are the molecular weight and mass density of $Li_2O_2$, and $\sigma_{eff}$ is the effective conductivity of electrons in the cathode, which is assumed to be:

$$\sigma_{eff} = \varepsilon^{\beta_e}\sigma, \tag{11}$$

where $\beta_e$ is the Bruggeman coefficient for the electron conductivity and $\sigma$ is the electron conductivity in the carbon electrode. The oxygen mass consumption is given by:

$$\frac{dm_{O_2}}{dt} = \frac{M_{O_2}}{2F} I, \tag{12}$$

where $M_{O_2}$ is the molecular mass of $O_2$ and $I_{app}$ is the total current density at the cathode.

In order to establish the equation for the oxygen conversion rate $R_C$ one has to take into consideration the geometry of the electrolyte/carbon interface at the cathode, since this interface represents the active region where the lithium oxidation takes place. One model that is often used in the literature is to consider that the cathode contains a large number of quasi-cylindrical open-ended pores, each of average pore radius $\overline{r}_p$. The lithium peroxide deposits on the inner surface of the pores (see Fig. 2) and, in this way, decreases the average pore radius in time. If the shape of the pores is cylindrical, one can show that the porosity can be related to the average pore radius by:[6]

$$\varepsilon = \varepsilon_0 \left( \frac{\overline{r}_p}{\overline{r}_{p,0}} \right)^2, \tag{13}$$

where $\varepsilon_0$ and $\overline{r}_{p,0}$ are the initial porosity and average pore radius (at $t = 0$). Using the same assumption about the shape of the pores, the oxygen conversion rate can be approximated as:

$$R_C = \begin{cases} \dfrac{2k\varepsilon_{O_2} c_{O_2}}{\overline{r}_p c_{O_2}^{ref}} \times \left[ e^{\frac{(1-\beta)F}{RT}\eta_c} - e^{-\frac{\beta F}{RT}\eta_c} \right] & \text{if } L_C < x < L \text{ (cathode)} \\ 0, \text{ otherwise} \end{cases} \tag{14}$$

where $\beta = 0.5$, $k$ is a reaction rate constant, $c_{O_2}^{ref} = 1$ mol/l is a normalization parameter, and $\eta_c$ is the overpotential at the cathode. If we take into consideration the electrical resistivity of the $Li_2O_2$, which is assumed to deposit uniformly on the inner surface of the pores, the overpotential can be written as:

$$\eta_c = \phi_{Li} - \phi - U_c - \Delta V_{Li_2O_2} = \phi_{Li} - \phi - U_c - \frac{R_C \rho_{Li_2O_2} \overline{r}_{p,0}^2}{2\varepsilon_0} \ln \sqrt{\frac{\varepsilon_0}{\varepsilon}}, \tag{15}$$

where $\Delta V_{Li_2O_2}$ is the voltage drop across the $Li_2O_2$, $\rho_{Li_2O_2}$ is the electrical resistivity of the $Li_2O_2$, and $U_c$ is the equilibrium potential for reaction (1) at the cathode.

Equations (2)-(4), (9), (10), and (12) represent a system of partial differential equations that should be subject to boundary and initial conditions and solved self-consistently in order to compute the lithium-ion and oxygen concentrations, the electrostatic potentials, and the porosity at each location inside the electrochemical cell as a function of time. The initial conditions as well as the boundary conditions for the one-dimensional cell simulated in this article are presented in the next two subsections.

*Initial conditions*—Initial conditions are be specified for the lithium-ion and oxygen concentrations, porosity, and average pore radius at each location inside the device. The values of all initial parameters are detailed in Table 1. It is important to note that during a short time interval, immediately after one applies a current through the battery, the battery will consume the oxygen that is already stored in the cathode. This phenomenon is due to the fact that the initial $O_2$ concentration is relatively high inside the cathode (and equal to $c_{O_2,0}$), and the diffusion coefficient of $O_2$ is usually much smaller than the diffusion coefficient of $Li^+$. After a relatively short discharge time (typically of the order of seconds) the battery enters a quasi-stationary regime in which $O_2$ is provided by the outside atmosphere. To estimate the time $\tau$ required to deplete the initial $O_2$ from the cathode one can assume that the first term in the right-hand side of eq. (4) is much smaller than the other terms and write $\frac{\Delta\left(\varepsilon c_{O_2}\right)}{\tau} = -\frac{R_C}{2F}$, which gives:

$$\tau = \frac{2F\varepsilon_0 c_{O_2,0}\left(L - L_C\right)}{I} \approx 0.63 \frac{\varepsilon_0\left(L - L_C\right)}{I}, \tag{16}$$

where $I$ is the discharge current and $L-L_C$ is the length of the cathode (see Fig. 1). $\tau$ is expressed in seconds, $L$ and $L_C$ are expressed in cm, and $I$ is expressed in A/cm$^2$. In deriving (16) we have assumed that the porosity is not changing significantly during time $\tau$ and used the fact that $I = R_C\left(L-L_C\right)$. The specific capacity $SC_\tau$ (measured in mAh/g) required to deplete the initial $O_2$ from the cathode is:

$$SC_\tau = \frac{Fc_{O_2,0}\varepsilon_0}{1.8\rho_C\left(1-\varepsilon_0\right)} \approx 0.077\frac{\varepsilon_0}{1-\varepsilon_0}. \tag{17}$$

*Boundary conditions*—Boundary conditions are imposed for the $Li^+$ and oxygen concentrations and potentials, and for the electron potential at the cathode. The oxygen concentration at the right side of the cathode (i.e. at $x = L$) is assumed constant and can be computed from the oxygen solubility *s* and the external oxygen concentration $c_{O_2,ext}$ (see Table 1):

$$c_{O_2}\Big|_{x=L} = c_{O_2,0} = sc_{O_2,ext}. \tag{18}$$

The boundary condition at the anode is assumed to be:

$$\boldsymbol{I}_{c_{O_2}}\Big|_{x=0} = 0, \tag{19}$$

where $\boldsymbol{I}_{c_{O_2}} = -D_{O_2,eff}\nabla c_{O_2}$. The lithium concentration at the anode (i.e. $x = 0$) can be approximated by:

$$c_{Li}\left(x=0\right) = c_{Li,0}, \tag{20}$$

while at the cathode boundary satisfies:

$$\boldsymbol{I}_{c_{Li}}\Big|_{x=L} = 0, \tag{21}$$

where $\boldsymbol{I}_{c_{Li}} = -D_{Li,eff}\nabla c_{Li}$. A better approximation for Eq. 20 is to use the Newman boundary condition; however, since the electrolyte concentration is relatively constant in Li-air batteries, Eq. 20 is relatively accurate.

The potential for the Li transport equation (2) at the right side of or the cathode is:

$$\boldsymbol{I}_{Li}\big|_{x=L} = 0, \tag{22}$$

while at the anode it is calculated from the following rate equation:

$$\boldsymbol{I}_{Li}\big|_{x=0} = -R_A = -I_0\left(e^{\frac{(1-\beta')F}{RT}\eta_a} - e^{-\frac{\beta' F}{RT}\eta_a}\right), \tag{23}$$

where $\beta' = 0.5$, $I_0$ is a reaction rate constant, and $\eta_a$ is the overpotential at the anode reaction, which is equal to:

$$\eta_c = \phi - \phi_{Li} - U_a, \tag{24}$$

where $U_a$ is the equilibrium potential for the lithium reduction. The values of $s$, $c_{O_2,ext}$, $c_{Li,0}$, and $I_0$ are also reported in Table 1.

The electrostatic potential of the electrons at the right side of the cathode is equal to the applied external potential on the cathode electrode. The boundary condition for the electron conduction equation (9) at the cathode-separator interface is

$$\boldsymbol{I}_e\big|_{x=L_C} = 0, \tag{25}$$

where $\boldsymbol{I}_e = -\sigma_{eff}\nabla\phi$. The electron current at the right side of the cathode is equal to the value of the applied current.

Continuous boundary conditions are assumed for all density current variables at the anode/separator and cathode/separator interfaces (i.e. $\boldsymbol{I}_{Li}\big|_{x=L_C^+} = \boldsymbol{I}_{Li}\big|_{x=L_C^-}$, $\boldsymbol{I}_{c_{O_2}}\Big|_{x=L_A^+} = \boldsymbol{I}_{c_{O_2}}\Big|_{x=L_A^-}$, etc.).

The voltage of the cell is calculated as the difference of the electron potential at the cathode and the lithium-ion potential at the anode side, $V_{cell} = \phi(x = L) - \phi_{Li}(x = 0)$.

*Maximum specific capacity*—The maximum specific capacity is achieved when the pores of the cathode are filled in entirely. In this case the total lifetime of the battery ($T$) can be derived from (10) which becomes $\frac{\Delta\varepsilon}{T} = -R_C \frac{M_{Li_2O_2}}{2F\rho_{Li_2O_2}}$, or:

$$T = \frac{2F\rho_{Li_2O_2}\varepsilon_0(L - L_C)}{IM_{Li_2O_2}} \approx 9001\frac{\varepsilon_0(L - L_C)}{I}. \quad (26)$$

The corresponding maximum specific capacity $SC_{\max}$ expressed in mAh/g is given by:

$$SC_{\max} = \frac{\varepsilon_0 F\rho_{Li_2O_2}}{1.8(1-\varepsilon_0)\rho_C M_{Li_2O_2}} \approx 1104\frac{\varepsilon_0}{1-\varepsilon_0}. \quad (27)$$

In the last two equations $T$ is expressed in seconds, $L$ and $L_C$ are expressed in cm, and $I$ is expressed in A/cm$^2$. Eq. (27) shows that the maximum specific capacity of a Li-air battery with organic electrolyte and $\varepsilon_0 = 75\%$ is approximately 3,312 mAh/$g_C$, which agrees with other estimations from the literature.[3]

*Numerical implementation*—The transport equations and the boundary conditions presented above have been discretized by using finite differences in the case of one-dimensional battery systems. The nonlinear discretized equations have been implemented in RandFlux[11] and solved by using the Newton iterative technique. The specific capacity of the battery is computed by solving the transport equations till the porosity of at least one mesh point becomes zero. The energy density is computed by integrating numerically $I(t)V(t)$ from 0 to the lifetime of the battery. The power density is computed by dividing the energy density to the total lifetime of the

battery. The computational time required to compute the power and energy densities is of the order of 1 min on a standard one-processor computer running at 3 MHz.

*Parameter selection*—The selection of model parameters is critical for the accurate simulation of the Li-air battery. The values of the geometrical and material parameters used in simulations and the references from which they were taken are reported in Table 1. The parameters without a reference have been calibrated against experimental data published in the literature as described below.

The initial porosities of the cathode and separator were taken equal to 75%, which is in agreement to the actual values in current batteries. Since the thicknesses of the APL and separator are much smaller than the thickness of the cathode, the exact values of the oxygen and lithium diffusion coefficients, and the transference numbers in these regions do not affect significantly the results of the simulations. Most of these coefficients were considered to be either equal or larger than their values in the cathode's electrolyte. The reaction rate constant at the anode was estimated in order to obtain the best agreement between the results of our simulations and the experimental values of the cell voltage as a function of the specific capacity published in the literature.[5]

## Simulation results

Figure 3 presents the oxygen and lithium concentrations ($c_{O_2}$ and $c_{Li}$), the electrostatic potential of electrons in carbon ($\phi$), and the potential of Li ions ($\phi_{Li}$) computed "shortly" after the battery starts discharging, when the quasi-stationary regime is obtained (see eq. (16)). Our simulations show that the quasi-stationary regime is obtained within less than 1 second after the

battery starts discharging for a discharge current of more than 0.1 mA/cm$^2$. The porosity when the quasi-stationary regime is obtained is almost uniform throughout the cathode and approximately equal to the initial value of 75%. While the battery is discharged, the porosity decreases at the right side of the cathode to zero, thus interrupting the incoming flow of oxygen in the cell.

Figure 4 shows the dependence of the voltage of the cell as a function of the specific capacity for different current densities. As expected, the voltage of the cell is larger for smaller discharge currents and the maximum specific capacity of the cell is increasing with the discharge current, that is consistent with experimental results obtained by different groups.[5, 12, 13] The inset in Fig. 4 shows the voltage of the cell during the time when the quasi-stationary regime is obtained, fact which was also observed in experiments.[4, 13] Figure 5 presents the cell voltage as a function of the specific capacity for different cathode thicknesses ranging from 33 μm to 3.3 mm (the cathode thickness is defined as $L - L_C$, as shown in Fig. 1). Note that specific capacity of the cell approaches the maximum limit given by eq. (27) because, for narrow cathodes, the oxygen can diffuse completely throughout the whole cathode volume. It can also be seen that the cell voltage decreases with decreasing the thickness of the cathode electrode. This is because in the case of batteries with smaller cathode thickness, there is less surface area available and the overpotential at the cathode as expressed by Eqn. (14) becomes higher. The specific capacity in Figs. 4 and 5 as well as in the other figures in this section is expressed in mAh/g$_c$ where the mass includes only the mass of the carbon in the cathode.

The porosity as a function of the position inside the cell is represented in Figure 6 for different states of discharge and at a discharge current of 0.1 mA/cm$^2$. Since the $O_2$ diffusion coefficient is much smaller than the Li diffusion coefficient, $Li_2O_2$ has deposited predominantly

at the air side of the cathode where the reaction rate is higher. This phenomenon decreases the total energy density of the cell and is regarded as one of the main disadvantages of Li-air batteries. It is apparent from these simulations that in order to improve the energy density of Li-air batteries one should either increase the diffusion coefficient of $O_2$ to make it comparable to the one of Li ions or increase the reaction rate at the left side of the cathode (near the separator) in order to efficiently fill in the pores of the cathode with $Li_2O_2$.

The dependence of the reaction rate as a function of the position inside the cell is represented in Fig. 7 for different states of discharge. Note that, while the battery discharges, the reaction rate decreases deep inside the cathode and increases at the surface of the cathode. This effect can be explained again based on the fact that the pores (channels) that provide oxygen to the cell are pinching off at the surface of the cell, thus decreasing the overall oxygen concentration deep inside the cathode. In the same time, the reaction rate is slightly higher at the surface of the cathode in order to conserve the total value of the current going through the battery, which equal to 0.1 $mA/cm^2$.

Figures 8 and 9 present the dependence of the oxygen and lithium concentrations respectively, as a function of position at different states of discharge and for different discharge currents. As expected, the oxygen concentration is maximum at the air side of the cathode and decreases significantly with the distance from the surface at air side, while the lithium concentration is slightly decreasing from the separator side to air side of the cathode.

The Ragone plot (energy vs. power density) is often used to characterize the energy and power densities of a battery. This plot is shown in Fig. 10 for the Li-air battery, in which each point is obtained for different discharge currents. The energy and power densities in Fig. 10 as well as in the other figures in this section are computed by considering only the mass of the

carbon and the initial mass of the electrolyte in the cathode. To compare with conventional Li-ion batteries, there are two notable differences: (1) the power density of Li-air battery is extremely low and (2) the energy density decreases rapidly with increasing the power density.

## Proposed new structures for high energy density

In this section a few structures that have the potential to improve the energy density of Li-air batteries are discussed. We focus on the possibility to use solvents with high oxygen solubility and diffusivity, catalysts with uniform and nonuniform distribution, and partly wetted air electrodes.

*Solvent with high oxygen solubility and/or diffusivity*—It has already been suggested in the literature that one of the factors that limit the energy and power densities of Li-air batteries is the relatively low diffusion coefficients of $O_2$.[4, 14] Hence, we investigate below the properties of these batteries under various solubility factors and diffusion coefficients of $O_2$ in the electrolyte. Fig. 11 presents the energy density, power density, and specific capacity of the battery as a function of the solubility of the $O_2$, *s*. Both the energy density and the specific capacity increase linearly with the solubility factor, however, the rate at which the power density is increasing seems to decrease with *s*. Fig. 12 presents the energy density, power density, and specific capacity of the battery as a function of the diffusion coefficients of $O_2$. It is interesting to note that, for normal values of the oxygen diffusion coefficient, the energy density, power density, and specific capacity are all increasing with the logarithm of $D_{O_2}$. The saturation at high values

of $D_{O_2}$ is due to the fact that, at these values, $D_{O_2}$ becomes comparable with $D_{Li}$, which becomes the new limiting factor.

*Catalysts with uniform distribution*—In order to investigate how the characteristics of the battery are changing with different reaction rate coefficients *k* we present the voltage of the cell as function of the specific capacity in Fig. 13. The energy density, power density, and specific capacity of the cell are represented in Fig. 14 as a function of the reaction rate coefficient *k.* This coefficient is assumed constant inside the cathode; the increase in the value of *k* models the addition of a uniformly distributed catalyst in the cathode. There is an increase in the power density of the cell for values of *k* up to $\sim 2\times10^{-6}$ A/cm$^2$ due to the reducing overpotential of cathode electrode, after which the power density saturates. In order to observe a significant increase in the energy density and specific capacity of the battery one has to increase the reaction rate to much higher values (larger than $\sim 2\times10^{-4}$ A/cm$^2$).

*Catalysts with nonuniform distribution*—It was mentioned before that because of the relatively low diffusion coefficient of $O_2$, $Li_2O_2$ deposits mostly at the edge of the cathode and interrupts the flow of the $O_2$ inside the cell. In order for the reaction product to deposit more or less uniformly throughout the cathode one needs to increase the reaction rate deep inside the cathode region and close to the cathode-separator interface. One way to achieve this is to use a catalyst with nonuniform distribution inside the cathode. To model the effect of the catalyst we assume that the reaction rate coefficient *k* in eq. (14) depends exponentially on the location in the cathode according to the following equation:

$$k(x) = k_0 \left( \frac{k_{\max}}{k_0} \right)^{\frac{L-x}{L-L_C}}, \tag{28}$$

where $k_0$ is the value of the reaction rate coefficient at the edge of the cathode (i.e. $x = L$), $k_{\max}$ is the value of the reaction rate coefficient at the cathode-separator interface, $L$ is the length of the cell, and $L_C$ is the coordinate of the cathode-separator interface (see Fig. 1). Note that according to eq. (28) the reaction rate coefficient increases exponentially from the edge of the cell to the cathode-separator interface, where it has the maximum value of $k_{\max}$. Fig. 15 presents the cell voltage as a function of the specific capacity for different values of $k_{\max}$ ranging from $k_0 = 1.7 \times 10^{-8}$ A/cm$^2$ to $4.8 \times 10^{-6}$ A/cm$^2$. Fig. 16 presents the energy density, power density, and specific capacity of the battery as a function of the maximum value of $k_{\max}$.

It is important now to compare the characteristics of the Li-air batteries with uniform to nonuniform catalyst. The energy density, power density, and specific capacity for a battery filled uniformly with catalyst so that the reaction rate coefficient $k$ is constant and equal to $5 \times 10^{-5}$ A/cm$^2$ are 2060 Wh/Kg, 7.27 W/Kg, and 667 mAh/g, respectively. The same parameters for a battery filled in with nonuniform catalyst so that the reaction rate varies exponentially from $1.7 \times 10^{-8}$ A/cm$^2$ at the right side of the cathode to $5 \times 10^{-5}$ A/cm$^2$ at the cathode-separator interface are 2850 Wh/Kg, 6.86 W/Kg, and 995 mAh/g, respectively. Although we have used less catalyst in the battery with nonuniform distribution and the power density decreased approximately by 6%, the energy density and specific capacity increased more than 38% and 49% respectively. These simulations suggest that to increase the energy density of present Li-air batteries, it is desirable to create a cathode in which the reaction rate decreases from left to right

for at least a few orders of magnitude. This will slightly decrease the power density of the cell but will enhance considerably the energy density and specific capacity.

To understand why the energy density of batteries with nonuniform catalyst distribution is much larger than for batteries with uniform catalyst distribution we have represented the porosity as a function of position in Figure 17 for different specific capacities and at the same discharge current of 0.1 $mA/cm^2$. Although the $O_2$ diffusion coefficient is still much smaller than the $Li^+$ diffusion coefficient, the reaction rate coefficient deep inside the cathode is much larger than at the surface, which makes the lithium peroxide to deposit more uniformly inside the cathode.

In addition to using nonuniformly distributed catalysts, a few other techniques to increase the power density of Li-air batteries have emerged in the literature. Such techniques include adjusting the electrode porosity and catalyst reactivity distributions in order to maximize the material utilization in the air electrode or using multiple time-release catalysts as discussed by Williford and Zhang[15].

*Partly wetted air electrodes*—Other possibilities to increase the energy density of Li-air batteries are to use partly wetted cathodes. For instance, in Fig. 18(a), the left side of the cathode is filled with electrolyte while the oxygen side is filled with air. In this case $O_2$ can easily diffuse through the air and arrive in the wet region. The electrolyte is constrained to stay close to the separator because of surface tension of the liquid (i.e. capillary action). The radius of curvature of the electrolyte and the angle between the surface of the electrolyte and the carbon surface of the pores can be easily computed from the surface tension of the electrolyte and radius of pores. The $Li_2O_2$ that is formed as a result of reaction (1) will replace the electrolyte, which will be pushed slowly away from the separator. The thickness of the wetted region $d$ (see Fig. 18(a)) should be

much smaller than the diffusion length of $O_2$ in the electrolyte in order for the $O_2$ to penetrate easily inside this region and fill it in completely with $Li_2O_2$. If well designed, such as system could fully fill in the cathode with $Li_2O_2$ and, in this way, achieve the maximum theoretical energy density given by (27). One parameter of practical interest in this case is the diffusion length of the $O_2$ in the electrolyte, which is estimated below.

To derive an approximate formula for the diffusion length of $O_2$ in the electrolyte we note that, for normal values of the electric conductivity in carbon electrode ($\sigma_{eff}$), the electrostatic potential of electrons is almost constant and equal to the value of the cell's potential. Also the lithium-ion concentration and lithium and oxygen potentials do not change much with position inside the cell. For these reasons and by assuming that the porosity is constant equation (4) can be easily integrated in the stationary case. Indeed:

$$\frac{d}{dx}\left( D_{O_2,eff}\frac{dc_{O_2}}{dx}\right)-\frac{k\varepsilon_{O_2}c_{O_2}}{F\overline{r}_p c_{O_2}^{ref}}\times\left[ e^{\frac{(1-\beta)F}{RT}\eta_c}-e^{-\frac{\beta F}{RT}\eta_c}\right]=0, \tag{29}$$

where $\eta_c=\phi_{Li}-\phi-U\approx$ constant (does not depend on $x$); if we consider that the oxygen diffusion coefficient does not depend on $x$ and denote $A=\frac{k\varepsilon_{O_2}}{F\overline{r}_p c_{O_2}^{ref}}\times\left[ e^{\frac{(1-\beta)F}{RT}\eta_c}-e^{-\frac{\beta F}{RT}\eta_c}\right]$ we obtain:

$$c_{O_2}=c_{O_2}^0\exp\left(-\frac{Ax}{D_{O_2,eff}}\right). \tag{30}$$

Parameter $A$ can be computed as function of the total current density of the cell $I=-2D_{O_2,eff}\frac{dc_{O_2}}{dx}$ where factor 2 appears because each molecule of $O_2$ will create 2 electrons. Combining the last two equations we obtain that:

$$c_{O_2} = c_{O_2}^0 \exp\left( -\frac{Ix}{2qN_A c_{O_2}^0 D_{O_2,eff}} \right), \tag{31}$$

which shows that the diffusion length of the oxygen is equal to:

$$\lambda = 2F\varepsilon^{1.5} \frac{c_{O_2}^0 D_{O_2}}{I}. \tag{32}$$

A similar equation to (32) but which does not include the porosity has been obtained by Reed et al.[4] Eq. (32) can be used to estimate the optimum thickness of the cathode of Li-air batteries. For instance, for a battery operating at a discharge current of 0.1 mA/cm$^2$, initial cathode porosity of 75%, external pressure of the atmosphere of 1 atm, and $O_2$ diffusion coefficient of $7\times10^{-6}$ cm$^2$/s, the cathode thickness in normal Li-air batteries or the thickness $d$ of the wetted part of the cathode should be of the order of $\lambda = 0.29$ mm.

Another partly wetted structure that has the potential to increase the energy density of Li-air batteries is represented in Fig. 18(b). The air can penetrate easily through the pores on the cathode and, then, diffuse through the thin layer of electrolyte whose thickness is much smaller than $\lambda$. The disadvantage of using this structure is that the electrolyte-to-air surface is large, which can make the electrolyte to evaporate easily. However, the advantage is that this structure has a relatively large power density due to the large electrolyte-to-air surface.

## Conclusion

A drift-diffusion based model was developed and used to analyze the limitations of Li-air batteries with organic electrolyte. The model uses the theory of concentrated solutions and takes into consideration the diffusion of the $O_2$, the electric conductivity of electrons in the cathode, the diffusion and conductivity of Li ions in the cell, the reaction rates at the anode and cathodes, and the formation of the lithium peroxide. The model can accurately predict the effects of the

pore radius, geometric dimensions, oxygen partial pressure, and various material parameters on the specific capacity, energy density, and power density of the battery.

## Acknowledgements

This work was supported by US Army-CERDEC.

## References


1. K. M. Abraham and Z. Jiang, *Journal of the Electrochemical Society*, **143**, 1 (1996).
2. I. Kowaluk, J. Read and M. Salomon, *Pure Appl Chem*, **79**, 851 (2007).
3. J. P. Zheng, R. Y. Liang, M. Hendrickson and E. J. Plichta, *Journal of the Electrochemical Society*, **155**, A432 (2008).
4. J. Read, K. Mutolo, M. Ervin, W. Behl, J. Wolfenstine, A. Driedger and D. Foster, *Journal of the Electrochemical Society*, **150**, A1351 (2003).
5. J. Read, *Journal of the Electrochemical Society*, **149**, A1190 (2002).
6. S. S. Sandhu, J. P. Fellner and G. W. Brutchen, *Journal of Power Sources*, **164**, 365 (2007).
7. G. G. Botte, V. R. Subramanian and R. E. White, *Electrochimica Acta*, **45**, 2595 (2000).
8. M. Doyle, T. F. Fuller and J. Newman, *Journal of the Electrochemical Society*, **140**, 1526 (1993).
9. V. R. Subramanian, V. Boovaragavan and V. D. Diwakar, *Electrochemical and Solid State Letters*, **10**, A255 (2007).
10. J. Newman and K. Thomas-Alyea, *Electrochemical Systems*, John Wiley&Sons (2004).
11. RandFlux, p. User manual v. 0.7, User's manual v.0.7, Florida State University, http://www.eng.fsu.edu/ms/RandFlux.
12. X. H. Yang, P. He and Y. Y. Xia, *Electrochemistry Communications*, **11**, 1127 (2009).
13. G. Q. Zhang, J. P. Zheng, R. Liang, C. Ahang, B. Wang, M. Hendrickson and E. J. Plichta, *Submitted to J. Electrochem. Soc.* (2010).
14. S. S. Sandhu, G. W. Brutchen and J. P. Fellner, *Journal of Power Sources*, **170**, 196 (2007).
15. R. E. Williford and J. G. Zhang, *Journal of Power Sources*, **194**, 1164 (2009).
16. D. R. Lide, *CRC Handbook of Chemistry and Physics*, CRC Press (2008).
17. S. G. Stewart and J. Newman, *Journal of the Electrochemical Society*, **155**, F13 (2008).
18. W. Xu, J. Xiao, J. Zhang, D. Y. Wang and J. G. Zhang, *Journal of the Electrochemical Society*, **156**, A773 (2009).
19. K. Xu, *Chem Rev*, **104**, 4303 (2004).
20. A. Nyman, M. Behm and G. Lindbergh, *Electrochimica Acta*, **53**, 6356 (2008).
21. H. Y. Wu, H. Zhang, X. L. Cheng and L. C. Cai, *Physics Letters A*, **360**, 352 (2006).

**Table I. Parameters used in simulations.**

| | Parameter | Value | Reference |
|---|---|---|---|
| **General parameters** | Molecular weight of Li ($M_{Li}$) | 6.941 g/mol | [16] |
| | Molecular weight of $O_2$ ($M_{O2}$) | 32 g/mol | [16] |
| | Initial pore radius ($\overline{r}_{p,0}$) | 20 nm | |
| | Cell open-voltage potential ($U_c + U_a$) | 2.959 V | [2] |
| | $\beta_{Li}$ | 2.5 | |
| | $\beta_{O2}$ | 3 | |
| | $\beta$ | 1.5 | |
| | Temperature ($T$) | 300 K | |
| **APL specific parameters** | Li ion concentration at $x = 0$($c_{Li,0}$) | $10^{-3}$ mol/cm$^3$ | |
| | Li ion diffusion coefficient ($D_{Li}$) | | [17] |
| | Transference number ($t^+$) | 1 | |
| | Porosity ($\varepsilon$) | 100% | |
| | APL thickness ($L_A$) | 50 nm | |
| **Separator specific parameters** | Initial porosity ($\varepsilon_0$) | 75% | |
| | Li ion conductivity ($\kappa$) | | |
| | $O_2$ diffusion coefficient ($D_{O_2}$) | | |
| | Li diffusion coefficient ($D_{Li}$) | $3.018\times10^{-5}\exp\left(0.357c_{Li}\right)$ | [17] |
| | Transference number ($t^+$) | 1 | |
| | Separator thickness ($L_C - L_A$) | 50 μm | |
| **Cathode specific parameters** | Initial porosity ($\varepsilon_0$) | 75% | |
| | Electric conductivity of carbon electrode ($\sigma$) | 1 S/cm | |
| | Electric resistivity of $Li_2O_2$ ($\rho_{Li_2O_2}$) | 0 | |
| | Li ion conductivity ($\kappa$) | 11.41 mS/cm | [18] |

| | | |
|---|---|---|
| $O_2$ diffusion coefficient ( $D_{O_2}$ ) | $7\times10^{-6}\ cm^2/s$ | 4 |
| External oxygen concentration ( $c_{O_2,ext}$ in the air at 1 atm) | $9.46\times10^{-6}$ $cm^{-3}$ | |
| $\beta_e$ | 1 | |
| Solubility factor ( $s$ ) | 0.344982 | |
| Electrolyte mass density ( $\rho_e$ ) | 1.2 g/cm$^3$ | 19 |
| Carbon mass density ( $\rho_e$ ) | 2.26 g/cm$^3$ | |
| Li diffusion coefficient ( $D_{Li}$ ) | $3.018\times10^{-5}\exp\left(0.357c_{Li}\right)$ | 17 |
| Transference number ( $t^+$ ) | $0.4492-0.4717\frac{c_{Li}}{c_{ref}}+0.4106\frac{c_{Li}^2}{c_{ref}^2}-0.1287\frac{c_{Li}^3}{c_{ref}^3}$ | 20 |
| Molecular weight of $Li_2O_2$ ($M_{Li2O2}$) | 45.88 g/mol | 16 |
| Mass density of $Li_2O_2$ ($\rho_{Li2O2}$) | 2.14 g/cm$^3$ | 16, 21 |
| Mass density of C ($\rho_C$) | 2.26 g/cm$^3$ | 16 |
| Cathode thickness ( $L-L_C$ ) | 0.75 mm | |

**FIGURE CAPTIONS**

**Figure 1.** Li-air battery system showing the region that is discretized and simulated.

**Figure 2.** Modeling of the oxygen diffusion and $Li_2O_2$ formation in the porous carbon cathode.

**Figure 3.** Concentrations of $O_2$ and electrolyte, and electrostatic potential of $Li^+$ and electrons in the cell, at a discharge current of $I$ = 1 mA.

**Figure 4.** Cell voltage as a function of the specific capacity for different discharge currents.

**Figure 5.** Cell voltage as a function of the specific capacity for different cathode thicknesses: (a) 33 μm, (b) 65 μm, (c) 0.1 mm, (d) 0.2 mm, (e) 0.4 mm, (f) 0.75 mm, (g) 1 mm, and (h) 3.3 mm.

**Figure 6.** Local dependence of the porosity when the battery is fully charged (0 capacity), partly charged (1/4, 2/4, and 3/4 capacity) and nearly completely discharged (4/4 capacity).

**Figure 7.** Local dependence of the reaction rate when the battery is fully charged (0 capacity), partly charged (1/4, 2/4, and 3/4 capacity) and nearly completely discharged (4/4 capacity).

**Figure 8.** Local dependence of the oxygen concentration when the battery is fully charged (0 capacity), partly charged (1/4, 2/4, and 3/4 capacity) and nearly completely discharged (4/4 capacity).

**Figure 9.** Local dependence of the lithium concentration when the battery is fully charged (0 capacity), partly charged (1/4, 2/4, and 3/4 capacity) and nearly completely discharged (4/4 capacity).

**Figure 10.** Energy density vs. power density computed for different discharge currents.

**Figure 11.** Energy density, power density, and specific capacity as a function of the solubility factor of $O_2$.

**Figure 12.** Energy density, power density, and specific capacity as a function of the diffusion coefficient of $O_2$ in the electrolyte.

**Figure 13.** Cell voltage vs. specific capacity for different reaction rate coefficients, $k$. The reaction rate is assumed uniform inside the cathode and equal to (a) $k = 1\text{x}10^{-9}$ A/cm$^2$, (b) $k = 4\times10^{-9}$ A/cm$^2$, (c) $k = 1.6\times10^{-8}$ A/cm$^2$, (d) $k = 6.4\times10^{-8}$ A/cm$^2$, (e) $k = 2.56\times10^{-7}$ A/cm$^2$, (f) $k = 10^{-6}$ A/cm$^2$, (g) $k = 4.1\times10^{-6}$ A/cm$^2$, (h) $k = 1.64\times10^{-5}$ A/cm$^2$, (i) $k = 4.1\times10^{-5}$ A/cm$^2$, and (j) $k = 2.62\times10^{-4}$ A/cm$^2$.

**Figure 14.** Energy density, power density, and specific capacity as a function of the reaction rate coefficient, *k*.

**Figure 15.** Cell voltage vs. specific capacity for different distributions of the catalyst. The catalyst is assumed nonuniformly distributed inside the cathode, increasing exponentially from the right side of the battery towards the separator-cathode interface according to eq. (28). The maximum value of the reaction rate $k_{max}$ (which is obtained at the separator-cathode interface) is equal to (a) $k_{max} = 1.7\times10^{-8}$ A/cm$^2$, (b) $k_{max} = 3.15\times10^{-8}$ A/cm$^2$, (c) $k_{max} = 10^{-7}$ A/cm$^2$, (v) $k_{max} = 3.4\times10^{-7}$ A/cm$^2$, (e) $k_{max} = 4.74\times10^{-7}$ A/cm$^2$, and (f) $k_{max} = 1.64\times10^{-6}$ A/cm$^2$. The inset shows the distribution of the catalyst.

**Figure 16.** Energy density, power density, and specific capacity as a function of maximum value of the reaction rate $k_{max}$. The catalyst is assumed nonuniformly distributed inside the cathode, increasing exponentially from the right side of the battery towards the separator-cathode interface according to eq. (28).

**Figure 17.** Local dependence of the porosity when the battery is fully charged (0 capacity), partly charged (1/4, 2/4, and 3/4 capacity) and nearly completely discharged (4/4 capacity). The catalyst is assumed nonuniformly distributed inside the cathode, increasing exponentially from the edge of the battery towards the separator-cathode interface, where $k_{max} = 1.64\times10^{-6}$ A/cm$^2$.

**Figure 18.** Partly wet cathode structures proposed to increase the energy density of Li-air batteries.

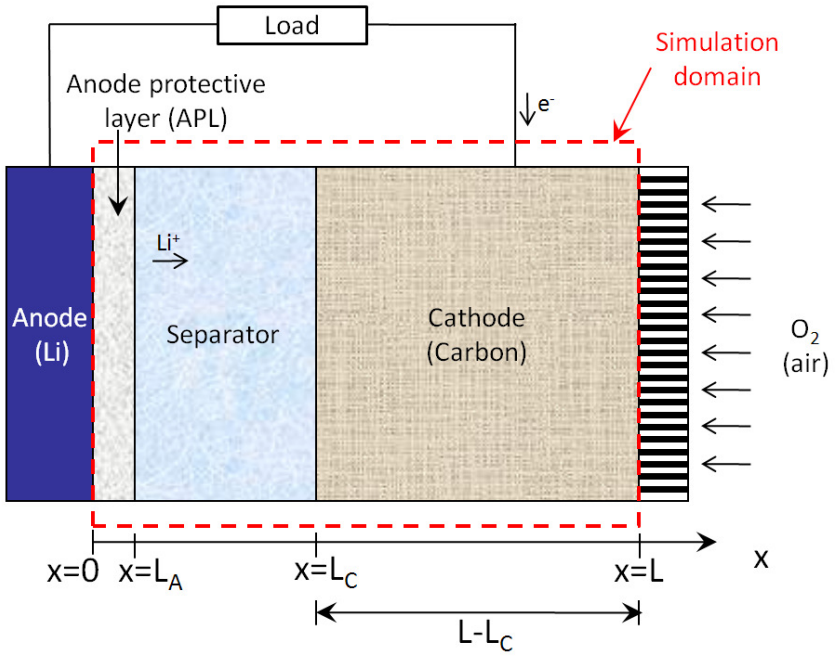


Figure 1.

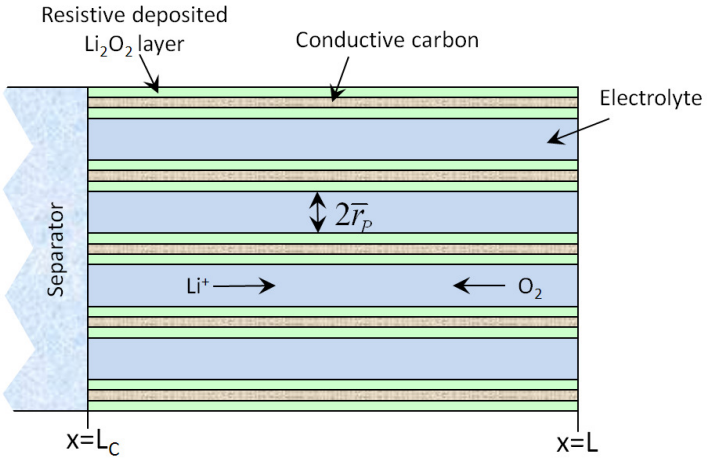


Figure 2.

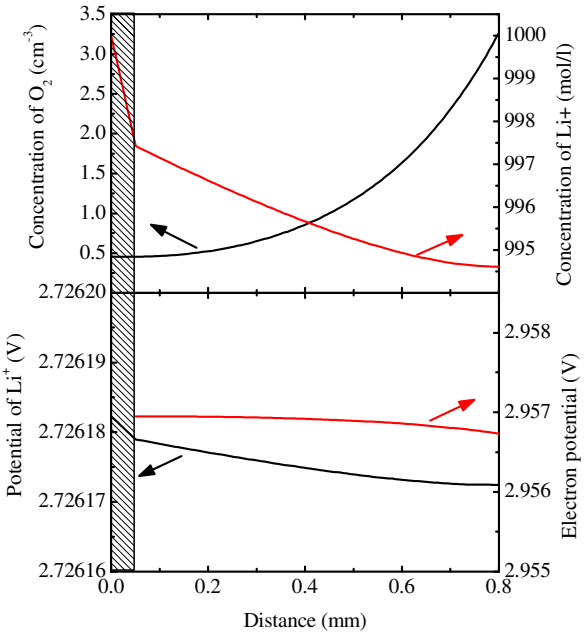


Figure 3.

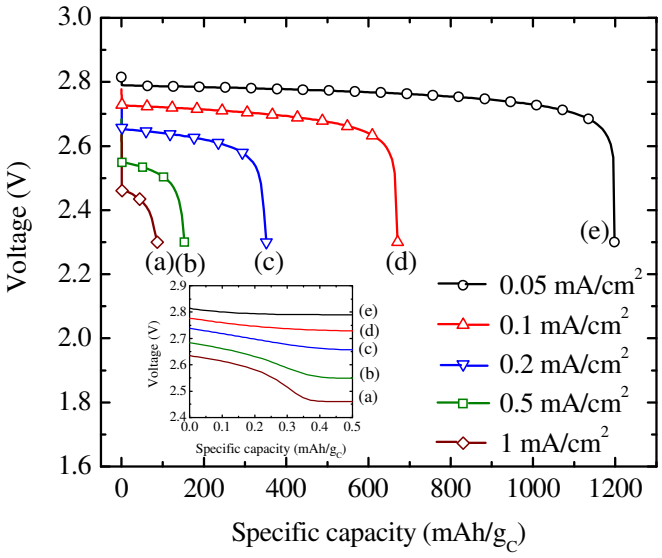


Figure 4.

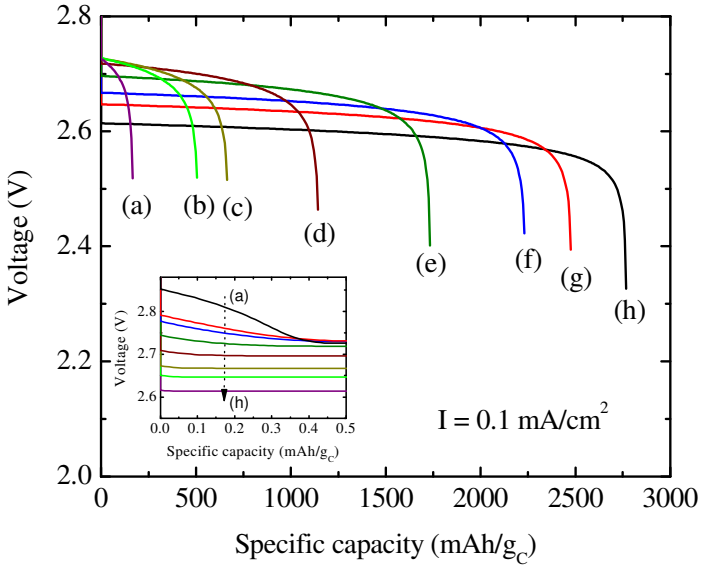


Figure 5.

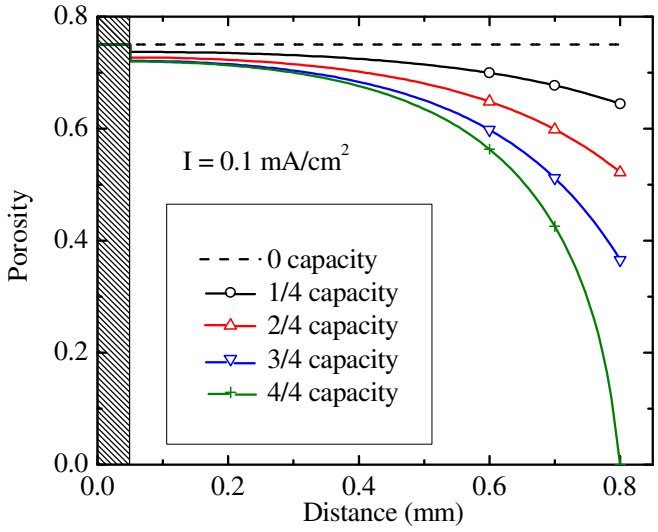


Figure 6.

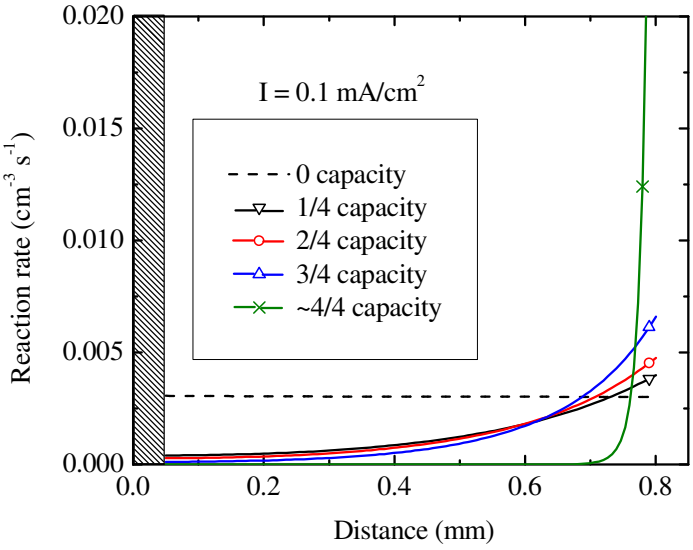


Figure 7.

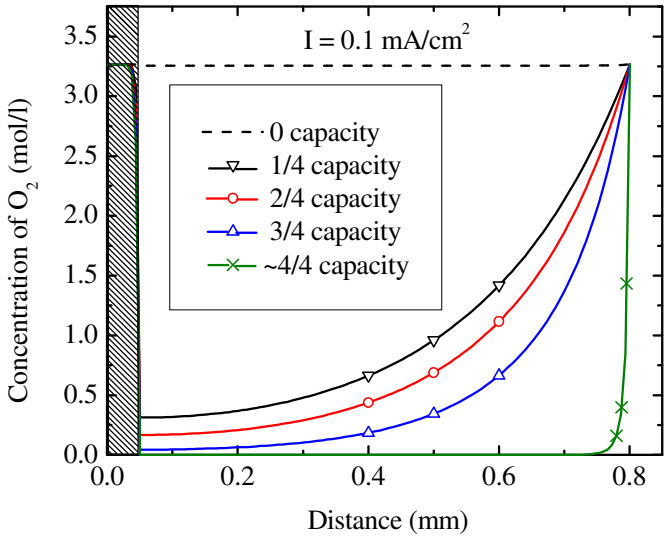


Figure 8.

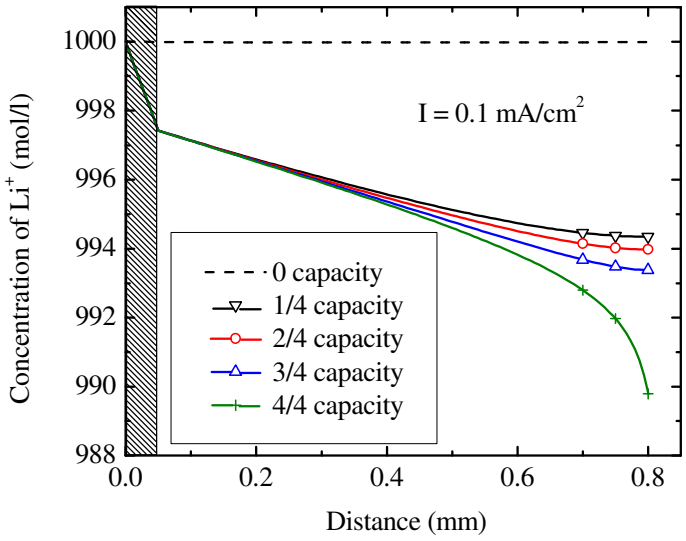


Figure 9.

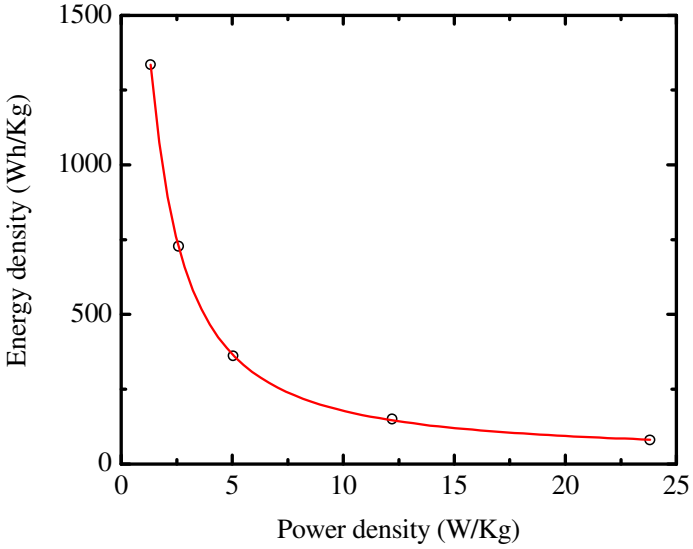


Figure 10.

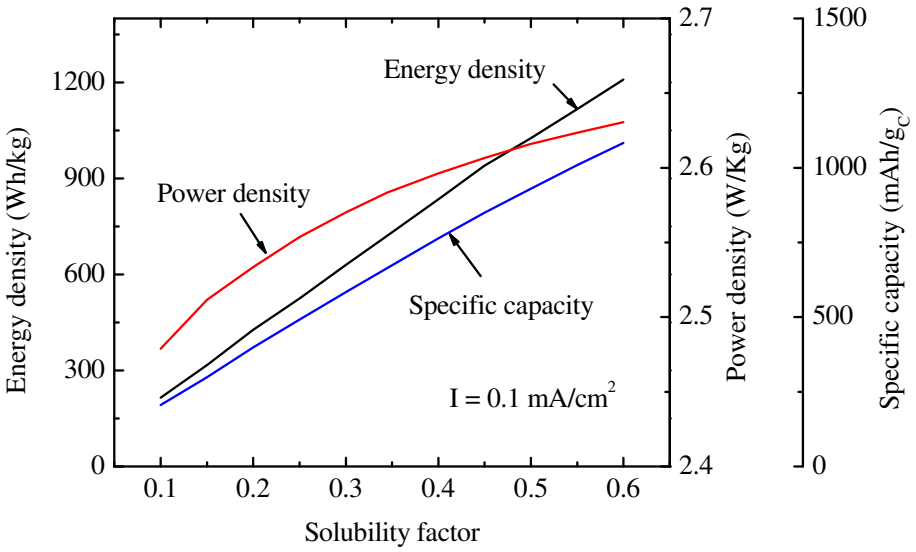


Figure 11.

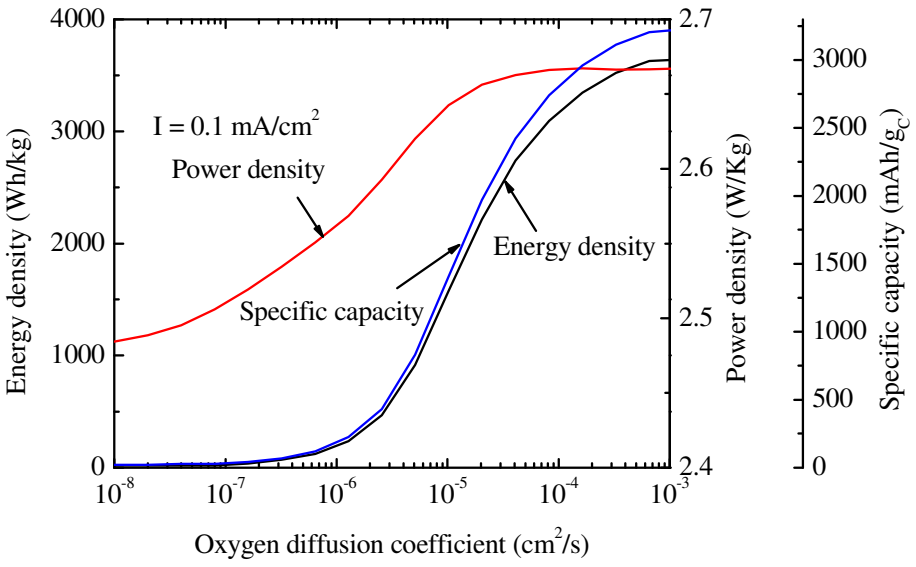


Figure 12.

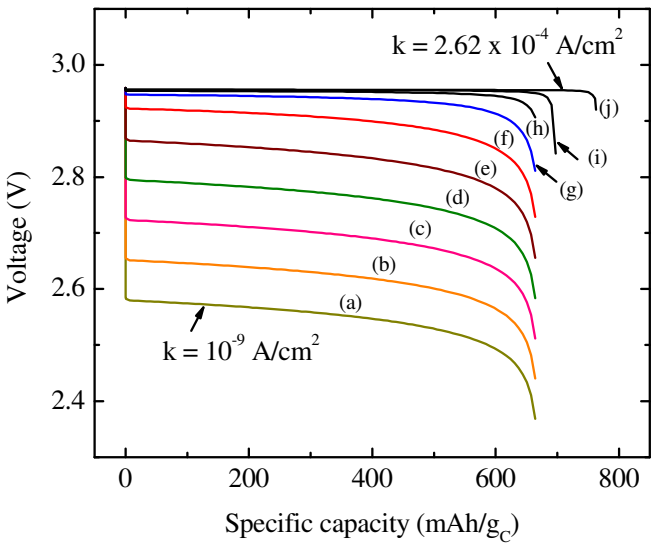


Figure 13.

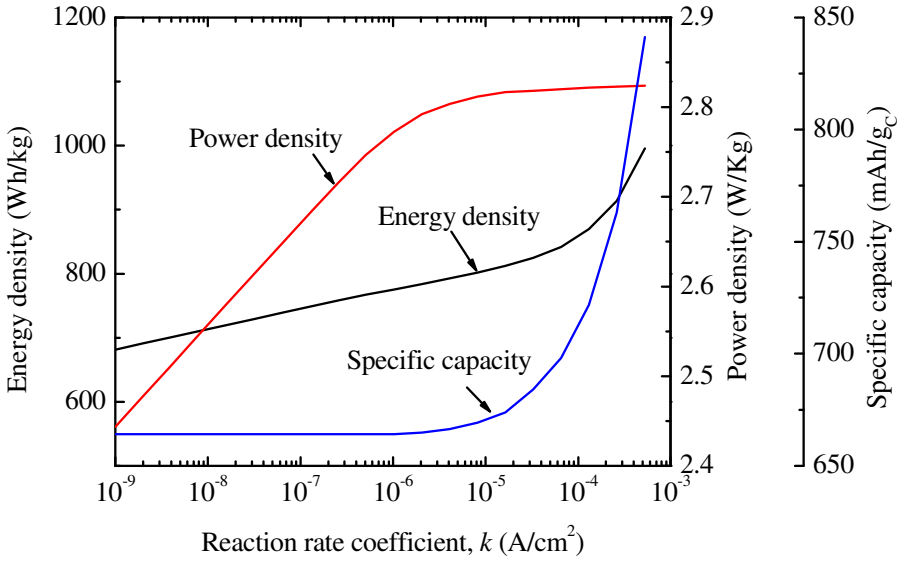


Figure 14

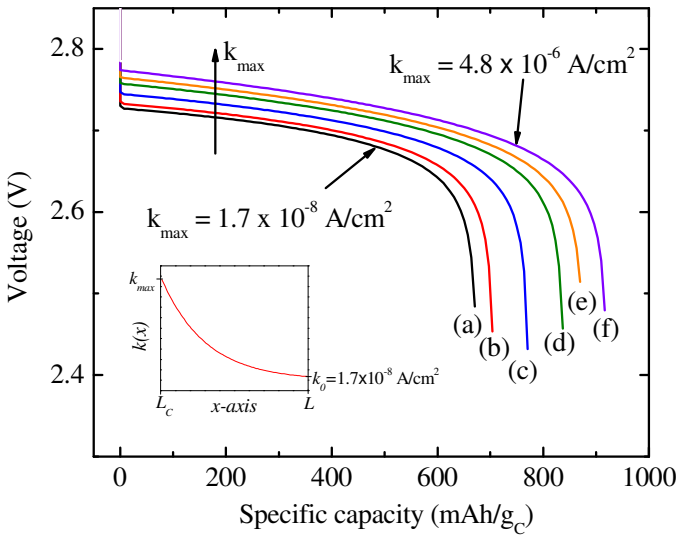


Figure 15

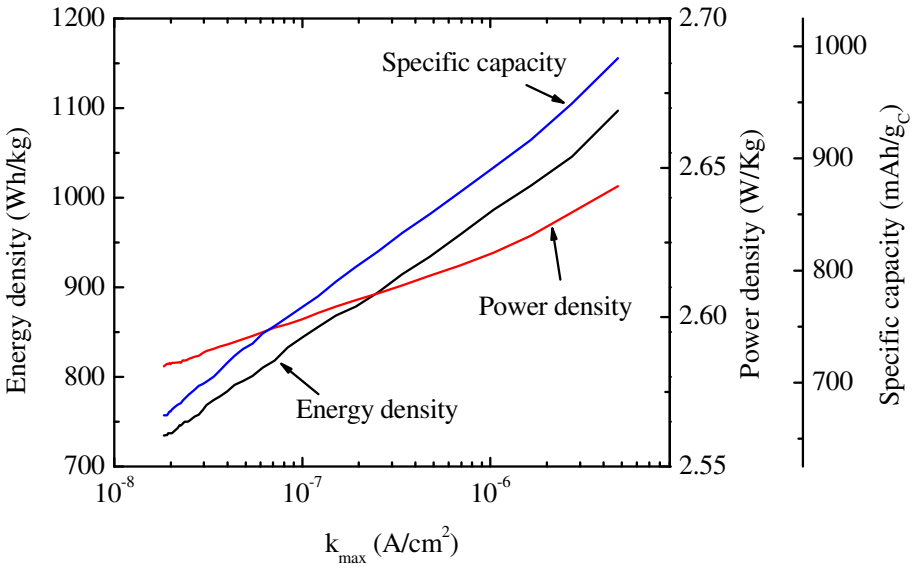


Figure 16

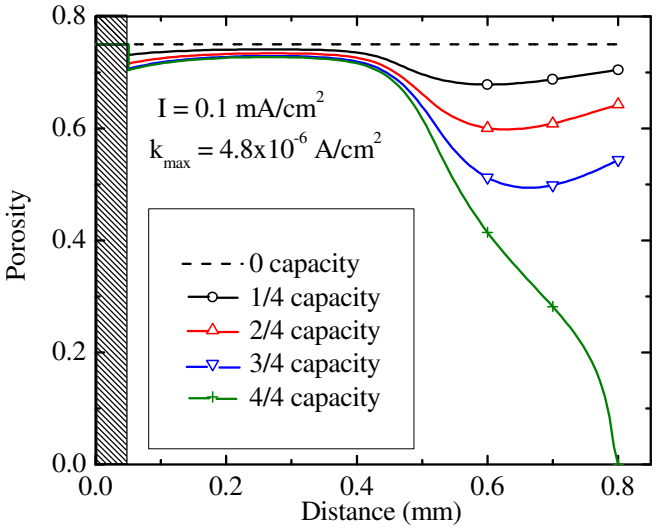


Figure 17

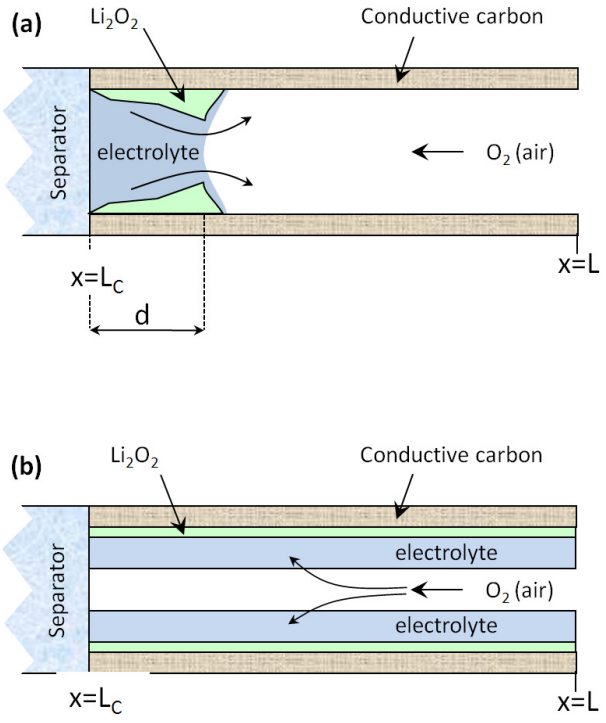


Figure 18